Group theoretical analysis of symmetry breaking in two-dimensional quantum dots

Constantine Yannouleas and Uzi Landman

School of Physics, Georgia Institute of Technology, Atlanta, Georgia 30332-0430, USA
(Received 18 December 2002; revised manuscript received 2 April 2003; published 28 July 2003)

We present a group theoretical study of the symmetry-broken unrestricted Hartree-Fock orbitals and electron densities in the case of a two-dimensional *N*-electron single quantum dot (with and without an external magnetic field). The breaking of rotational symmetry results in canonical orbitals that (1) are associated with the eigenvectors of a Hückel Hamiltonian having sites at the positions determined by the equilibrium molecular configuration of the classical *N*-electron problem and (2) transform according to the irreducible representations of the point group specified by the discrete symmetries of this classical molecular configuration. Through restoration of the total-spin and rotational symmetries via post-Hartree-Fock projection techniques, we show that the point-group discrete symmetry of the unrestricted Hartree-Fock wave function underlies the appearance of magic angular momenta (familiar from exact-diagonalization studies) in the excitation spectra of the quantum dot. Furthermore, this two-step symmetry-breaking and symmetry-restoration method accurately describes the energy spectra associated with the magic angular momenta.

I. INTRODUCTION

A. Background of the mean-field breaking of spatial symmetries in quantum dots

Two-dimensional (2D) quantum dots (QD's) created at semiconductor interfaces with refined control of their size, shape, and number of electrons are often referred[1–4] to as "artificial atoms." For high magnetic fields (*B*), it has been known for some time (ever since the pioneering work[5] of Laughlin in 1983 concerning the fractional quantum Hall effect) that 2D few-electron systems exhibit complex strongly correlated many-body physics. Nevertheless, for low magnetic fields, the term artificial atoms was used initially to suggest that the physics of electrons in such man-made nanostructures is exclusively related to that underlying the traditional description[6] of natural atoms (pertaining particularly to electronic shells and the Aufbau principle), where the electrons are taken[7] to be moving in a spherically averaged effective central mean field. This traditional picture was given support by experimental studies[3,4] on vertical QD's, which were followed[8] by a series of sophisticated theoretical investigations yielding results conforming to it.

However, in 1999, the circular (for 2D QD's) central-mean-field picture was challenged by the discovery of solutions with broken *space* symmetry in the context of spin-and-space unrestricted Hartree-Fock (sS-UHF) mean-field calculations.[9,10] These broken-symmetry (BS) solutions appear spontaneously (due to a phase transition) when the strength of the interelectron repulsion relative to the zero-point kinetic energy (R_W) exceeds a certain critical value. They indicate the formation of Wigner (or electron) molecules (WM's or EM's) with the electrons located at the vertices of nested regular polygons (often referred to as concentric rings), familiar from studies of classical point charges.[11,12] Such molecules were characterized by us as strong or weak Wigner crystallites depending on their rigidity or lack thereof (i.e., floppiness), suggesting the existence of additional[13] "phase transitions" as a function of the parameter R_W (see Sec. II B for its precise definition). Further-

more, it was noted[9] that the symmetry breaking should be accompanied by the emergence of a spectrum of collective rovibrational excitations (finite-size analogs of the Goldstone modes). A subsequent investigation[14] based on exact solutions for a helium QD (2e QD) confirmed these results and provided a systematic study of the molecular rovibrational collective spectra and their transition to independent particle excitations, as the rigidity of the WM was reduced through variation of the controlling parameter R_W.

We remark here that the lower-energy BS UHF solutions already capture[10] part of the correlation energy, compared to the restricted HF (RHF) ones. Improved numerical accuracy has been achieved in subsequent studies[15–17] through the restoration of the broken symmetries via projection techniques. Consequently, the methodology of symmetry breaking at the UHF mean-field level and of subsequent symmetry restoration via post Hartree-Fock methods[18] provides a systematic controlled hierarchy of approximations toward the exact solution, with anticipated advantages for complex many electron systems (under field-free conditions[15] and in the presence of a magnetic field[16,17]), whose treatment is computationally prohibitive with other methods (e.g., exact diagonalization).

B. Background of the mean-field breaking of symmetries in other finite-size fermionic systems

The mean-field approach has been a useful tool in elucidating the physics of small fermionic systems, from natural atoms and atomic nuclei to metallic nanoclusters and, most recently, of two-dimensional quantum dots. Of particular interest for motivating the present work (due to spatial-symmetry-breaking aspects) has been the mean-field description of deformed nuclei and metal clusters (exhibiting ellipsoidal shapes). At a first level, deformation effects in these systems can be investigated via semiempirical mean-field models, like the particle-rotor model[19] of Bohr and Mottelson (nuclei), the anisotropic-harmonic-oscillator model of Nilsson (nuclei[20] and metal clusters[21]), and the

shell-correction method of Strutinsky (nuclei[22] and metal clusters[23,24]). At the microscopic level, the mean field is often described[25,26] via the self-consistent single-determinantal HF theory. At this level, however, the description of deformation effects mentioned above requires[25,27] consideration of unrestricted Hartree-Fock wave functions that break explicitly the rotational symmetries of the original many-body Hamiltonian, but yield HF determinants with lower energy compared to the symmetry-adapted restricted Hartree-Fock solutions.

In earlier publications,[9,10,15–17] we have shown that, in the strongly correlated regime, UHF solutions violating the rotational (circular) symmetry arise most naturally in the case of 2D single QD's and for both the cases of zero and high magnetic field.[28] Unlike the case of atomic nuclei, however, where symmetry breaking is associated with quadrupole deformations, spontaneous symmetry breaking in 2D QD's induces electron localization associated with the formation of WM's.

The violation in the mean-field approximation of the symmetries of the original many-body Hamiltonian appears to be paradoxical at a first glance. However, for the specific cases arising in nuclear physics and quantum chemistry, two theoretical developments have resolved this paradox. They are (1) the theory of restoration of broken symmetries via projection techniques[29,30] and (2) the group theoretical analysis of symmetry-broken HF orbitals and solutions in chemical reactions initiated by Fukutome,[31] who used of course the symmetry groups associated with the natural 3D molecules. Despite the different fields, the general principles established in these earlier theoretical developments have provided a wellspring of assistance in our investigations of symmetry breaking in QD's. In particular, the restoration of broken circular symmetry in the case of single QD's has already been demonstrated by us in three recent publications.[15–17,32]

C. Content of this paper

In the present paper, we will provide an in-depth group theoretical analysis of broken-symmetry UHF orbitals and electron densities (ED's) in the case of single parabolic QD's. We will show that such an analysis provides further support for our earlier interpretation concerning the spontaneous formation of collectively rotating electron (or Wigner) molecules (REM's). Indeed we will demonstrate deep analogies between the electronic structure of the WM and that of the natural 3D molecules. In particular, we will show that the breaking of rotational symmetry results in canonical UHF orbitals that are associated with the eigenvectors of a molecular-type Hückel Hamiltonian having ''atomic'' sites at positions specified by the equilibrium configuration of the classical N-electron problem; these ''atomic'' sites are localization sites for the electrons, and they do not imply the presence of a positive nucleus. Thus, in contrast to the fully delocalized and symmetry-adapted, independent-particle-model-type orbitals of the RHF, the BS UHF orbitals with the *same spin direction* resemble closely the molecular orbitals (MO's) formed by linear combinations of atomic orbitals (LCAO's), which are prevalent[33] in chemistry. (Naturally, the

LCAO behavior of the UHF orbitals with the same spin direction allows for a more precise understanding of the term ''electron localization'' used by us in previous publications.) An important conclusion of the present paper is that the BS UHF orbitals are not necessarily unique; what matters, in analogy with the LCAO-MO's of natural molecules, is that they transform according to the irreducible representations of the point group specified by the discrete symmetries of the classical equilibrium configuration.[11]

Our study leads to the following two main results: (i) in analogy with 3D natural molecules, the WM's can rotate and the restoration of the total-spin and rotational symmetries via projection techniques describes their lowest rotational bands (*yrast* bands[14,34]) in addition to the ground state and (ii) the lowering of the symmetry, which results in the (discrete) point-group symmetry of the UHF wave function, underlies the appearance of the sequences of magic angular momenta (familiar from exact-diagonalization studies[35–40]) in the excitation spectra of single QD's. Since exact-diagonalization methods are typically restricted to small sizes with $N \leqslant 10$, the present two-step method of breakage and subsequent restoration of symmetries offers a promising new avenue for accurately describing larger 2D electronic systems. A concrete example of the potential of this approach is provided by Ref. 16 and Ref. 17, where our use of the the symmetry-breaking and symmetry-restoration method yielded analytic expressions for correlated wave functions that offer a better description of the N-electron problem in high magnetic fields compared to the Jastrow-Laughlin[5] expression.

Since the group theoretical aspects of symmetry breaking at the mean-field level (and their relation to the properties of the exact solutions) remain a vastly unexplored territory in the area of condensed-matter finite-size systems, in the following we will present an introductory investigation of them through a series of rather simple, but nontrivial, illustrative examples from the field of 2D parabolic QD's. The plan of the paper is as follows: Section II reviews briefly the set of UHF equations employed by us; Secs. III and IV present the case of three electrons in the absence and in the presence of an external magnetic field B, respectively. The more complicated case of six electrons at $B=0$ is investigated in Sec. V, while Sec. VI discusses the companion step of the restoration of broken symmetries, which underlies the appearance of magic angular momenta in the exact spectra. Finally, Sec. VII presents a summary.

Before leaving the Introduction, we wish to stress that analogs of several of the group theoretical concepts and manipulations employed in this paper can be found in textbooks concerning standard applications of symmetry groups to the electronic structure and chemistry of 3D natural molecules. Here, however, we will use these otherwise well-known group theoretical aspects to elucidate the molecular interpretation of the BS UHF determinants (and associated orbitals) in the unexpected context of a newly arising area of physics: namely, the physics of strong correlations in 2D circular artificial atoms (QD's).

II. UHF EQUATIONS

A. Pople-Nesbet equations

The UHF equations we are using are the Pople-Nesbet[41] equations described in detail in Chap. 3.8 of Ref. 26. For

completeness, we present here a brief description of them, along with details of their computational implementation by us to the 2D case of semiconductor QD's.

The key point is that electrons of α (up) spin are described by one set of spatial orbitals $\{\psi_j^\alpha | j = 1,2, \ldots, K\}$, while electrons of β (down) spin are described by a different set of spatial orbitals $\{\psi_j^\beta | j = 1,2, \ldots, K\}$ (of course in the RHF $\psi_j^\alpha = \psi_j^\beta = \psi_j$). Next, one introduces a set of basis functions $\{\varphi_\mu | \mu = 1,2, \ldots, K\}$ (constructed to be *orthonormal* in our 2D case), and expands the UHF orbitals as

$$\psi_i^\alpha = \sum_{\mu=1}^K C_{\mu i}^\alpha \varphi_\mu, \quad i = 1,2, \ldots, K, \tag{1}$$

$$\psi_i^\beta = \sum_{\mu=1}^K C_{\mu i}^\beta \varphi_\mu, \quad i = 1,2, \ldots, K. \tag{2}$$

The UHF equations are a system of two coupled matrix eigenvalue problems

$$\mathbf{F}^\alpha \mathbf{C}^\alpha = \mathbf{C}^\alpha \mathbf{E}^\alpha, \tag{3}$$

$$\mathbf{F}^\beta \mathbf{C}^\beta = \mathbf{C}^\beta \mathbf{E}^\beta, \tag{4}$$

where $\mathbf{F}^{\alpha(\beta)}$ are the Fock-operator matrices and $\mathbf{C}^{\alpha(\beta)}$ are the vectors formed with the coefficients in the expansions (1) and (2). The matrices $\mathbf{E}^{\alpha(\beta)}$ are *diagonal*, and as a result Eqs. (3) and (4) are *canonical* (standard). Notice that noncanonical forms of HF equations are also possible (see Chap. 3.2.2 of Ref. 26). Since the self-consistent iterative solution of the HF equations can be computationally implemented only in their canonical form, heretofore canonical orbitals and solutions will always be implied, unless otherwise noted explicitly. We note that the coupling between the two UHF equations (3) and (4) is given explicitly in the expressions for the elements of the Fock matrices below [Eqs. (7) and (8)].

Introducing the density matrices $\mathbf{P}^{\alpha(\beta)}$ for $\alpha(\beta)$ electrons,

$$P_{\mu\nu}^\alpha = \sum_a^{N^\alpha} C_{\mu a}^\alpha (C_{\nu a}^\alpha)^* \tag{5}$$

$$P_{\mu\nu}^\beta = \sum_a^{N^\beta} C_{\mu a}^\beta (C_{\nu a}^\beta)^*, \tag{6}$$

where $N^\alpha + N^\beta = N$, the elements of the Fock-operator matrices are given by

$$F_{\mu\nu}^\alpha = H_{\mu\nu} + \sum_\lambda \sum_\sigma P_{\lambda\sigma}^\alpha [(\mu\sigma|\nu\lambda) - (\mu\sigma|\lambda\nu)]$$

$$+ \sum_\lambda \sum_\sigma P_{\lambda\sigma}^\beta (\mu\sigma|\nu\lambda), \tag{7}$$

$$F_{\mu\nu}^\beta = H_{\mu\nu} + \sum_\lambda \sum_\sigma P_{\lambda\sigma}^\beta [(\mu\sigma|\nu\lambda) - (\mu\sigma|\lambda\nu)]$$

$$+ \sum_\lambda \sum_\sigma P_{\lambda\sigma}^\alpha (\mu\sigma|\nu\lambda), \tag{8}$$

where $H_{\mu\nu}$ are the elements of the single-electron Hamiltonian with an external magnetic field B and an appropriate potential confinement, and the Coulomb repulsion is expressed via the two-electron integrals

$$(\mu\sigma|\nu\lambda)$$

$$= \frac{e^2}{\kappa} \int d\mathbf{r}_1 d\mathbf{r}_2 \varphi_\mu^*(\mathbf{r}_1) \varphi_\sigma^*(\mathbf{r}_2) \frac{1}{|\mathbf{r}_1 - \mathbf{r}_2|} \varphi_\nu(\mathbf{r}_1) \varphi_\lambda(\mathbf{r}_2),$$

$$\tag{9}$$

with κ being the dielectric constant of the semiconductor material. Of course, the Greek indices μ, ν, λ, and σ run from 1 to K.

For a QD, the external confinement is assumed to be parabolic, and the single-particle Hamiltonian in a perpendicular external magnetic field B is written as

$$H = \frac{(\mathbf{p} - e\mathbf{A}/c)^2}{2m^*} + \frac{1}{2} m^* \omega_0^2 (x^2 + y^2) + \frac{g^* \mu_B}{\hbar} \mathbf{B} \cdot \mathbf{s}. \tag{10}$$

The vector potential $\mathbf{A}$ is given in the symmetric gauge by

$$\mathbf{A}(\mathbf{r}) = \frac{1}{2} \mathbf{B} \times \mathbf{r} = \frac{1}{2}(-By, Bx, 0), \tag{11}$$

and the last term in Eq. (10) is the Zeeman interaction with g^* being the effective g factor, μ_B the Bohr magneton, and $\mathbf{s}$ the spin of an individual electron. m^* is the effective electron mass and ω_0 is the frequency parameter of the parabolic potential confinement.

The system of the two coupled UHF matrix equations (3) and (4) is solved self-consistently through iteration cycles.[42] For obtaining the numerical solutions, we have used a set of $K = 78$ basis states φ_i's that are chosen to be the product wave functions formed out from the eigenstates of the one-dimensional harmonic oscillators along the x and y axes. This basis is often referred to as "Real Cartesian harmonic oscillator basis." Note that the value $K = 78$ corresponds to all the states of the associated 2D harmonic oscillator up to and including the 12th major shell.

Having obtained the self-consistent solution, the total UHF energy is calculated as

$$E_{\text{UHF}} = \frac{1}{2} \sum_\mu \sum_\nu [(P_{\nu\mu}^\alpha + P_{\nu\mu}^\beta) H_{\mu\nu} + P_{\nu\mu}^\alpha F_{\mu\nu}^\alpha + P_{\nu\mu}^\beta F_{\mu\nu}^\beta]. \tag{12}$$

B. Solutions representing Wigner molecules

As a typical example of a solution that can be extracted from the above UHF equations, we mention the case of $N = 19$ electrons for $\hbar\omega_0 = 5$ meV, $R_W = 5$ ($\kappa = 3.8191$), and $B = 0$. The Wigner parameter $R_W \equiv Q/\hbar\omega_0$, where Q is the Coulomb interaction strength; $Q = e^2/\kappa l_0$, with $l_0 = (\hbar/m^*\omega_0)^{1/2}$ being the spatial extent of the lowest single-electron wave function in the parabolic confinement.

Figure 1 displays the total electron density of the BS UHF solution for these parameters, which exhibits breaking of the rotational symmetry. In accordance with ED's for smaller dot sizes published by us earlier,[9,10] the ED in Fig. 1 is highly
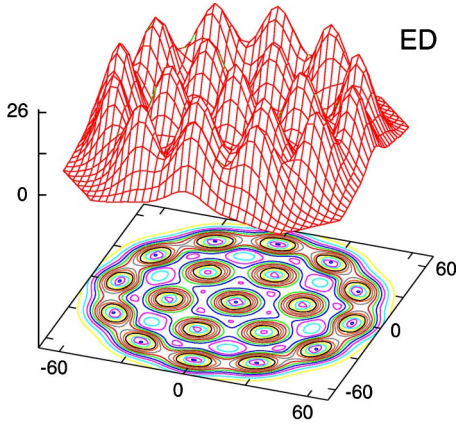
FIG. 1. UHF electron density in a parabolic QD for $N=19$ and $S_z=19/2$, exhibiting breaking of the circular symmetry at $R_W=5$ and $B=0$. The choice of the remaining parameters is $\hbar\omega_0 =5$ meV and $m^*=0.067m_e$. Distances (along the horizontal x and y axes) are in nanometers and the electron density (along the vertical axis) in 10^{-4} nm^{-2}.

suggestive of the formation of a Wigner molecule, with an (1,6,12) ring structure in the present case. This polygonal ring structure agrees with the classical one[11] and is sufficiently complex to instill confidence that the Wigner-molecule interpretation is valid. The following question, however, arises naturally at this point: is such a molecular interpretation limited to the intuition provided by the landscapes of the total ED's, or are there deeper analogies with the electronic structure of natural 3D molecules? The answer to the second part of this question is in the positive, and the remainder of this paper is devoted to discovering such analogies. However, since the $N=19$ case represents a rather complicated group theoretical structure, for simplicity and transparency, we will study in the following smaller QD sizes. This, however, will not result in any loss of generality in our conclusions.

In previous publications,[9,10] we found that *space* symmetry breaking in the UHF equations appears spontaneously for $R_W>1$. Below we choose to work with larger values of R_W (e.g., 10 or higher), for which the effects of strong correlations are fully developed. The group theoretical investigation of the intermediate regime near the phase transition is left for a future publication. In all calculated cases, we used $\hbar\omega_0 =5$ meV, $m^*=0.067m_e$ (GaAs), and $g^*=-0.44$ (GaAs).

We note that the Pople-Nesbet UHF equations are primarily employed in quantum chemistry for studying the ground states of open-shell molecules and atoms. Unlike our studies of QD's, however, such chemical UHF studies consider mainly the breaking of the total spin symmetry, and not that of the space symmetries. As a result, for purposes of emphasis and clarity, we have often used (see, e.g., our previous papers) prefixes to indicate the specific unrestrictions involved in our UHF solutions, i.e., the prefix s for the total spin and the prefix S for the space unrestriction.

C. Solutions representing pure spin density waves

Before leaving this section, we mention another class of BS solutions which can appear in single QD's; namely, the
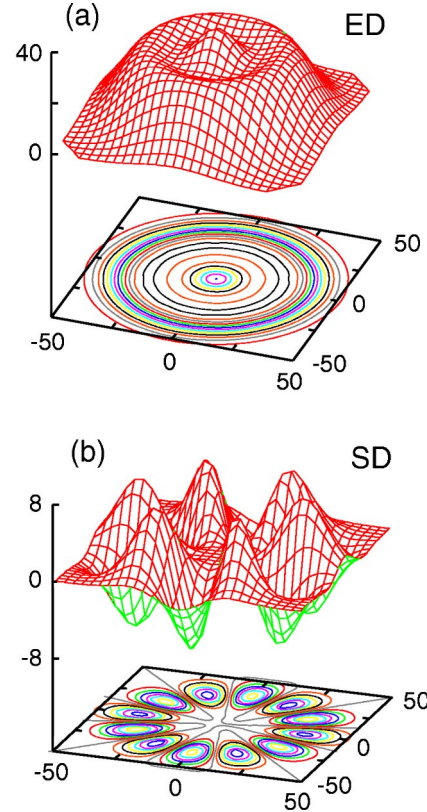

FIG. 2. UHF solution in a parabolic QD exhibiting a pure spin density wave for $N=14$, $S_z=0$, $R_W=0.8$, and $B=0$. (a) The total electron density exhibiting circular symmetry; (b) The spin density exhibiting azimuthal modulation (note the 12 humps whose number is smaller than the number of electrons). The choice of the remaining parameters is $\hbar\omega_0=5$ meV and $m^*=0.067m_e$. Distances are in nanometers and the electron and spin densities in 10^{-4} nm^{-2}.

spin density waves (SDW's). The SDW's are unrelated to electron localization and thus are quite distinct from the WM's; in single QD's, they were obtained[43] earlier within the framework of spin density functional theory.[44] To emphasize the different nature of SDW's and WM's, we present in Fig. 2 an example of a SDW obtained with the UHF approach [the corresponding parameters are $N=14$, $S_z=0$, $R_W=0.8$ ($\kappa=23.8693$), and $B=0$]. Unlike the case of WM's, the SDW exhibits a circular ED [see Fig. 2(a)], and thus does not break the rotational symmetry. Naturally, in keeping with its name, the SDW breaks the total-spin symmetry and exhibits azimuthal modulations in the spin density[45] (SD) [see Fig. 2(b); however, the number of humps is smaller than the number of electrons[46]]. The SDW's in single QD's appear for $R_W\lesssim1$ and are of lesser importance[47]; thus in the following we will exclusively study the case of WM's.

III. THREE ELECTRONS WITHOUT MAGNETIC FIELD

A. $S_z=3/2$ fully spin polarized case

We begin with the case of $N=3$ fully spin polarized ($S_z =3/2$) electrons in the absence of a magnetic field and for $R_W=10$ ($\kappa=1.9095$). Fully spin polarized UHF determi-
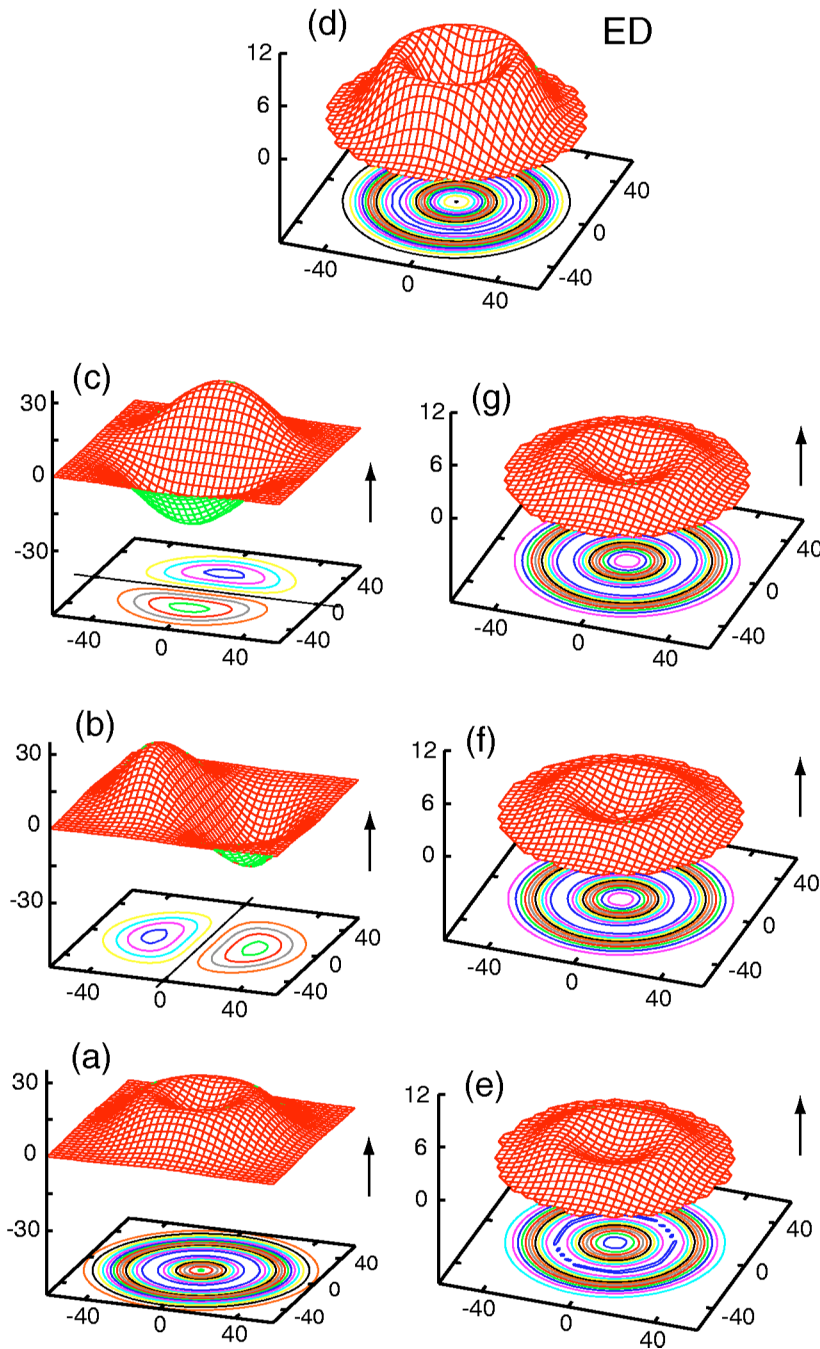
FIG. 3. The RHF case for $N=3$ and $S_z=3/2$ at $R_W=10$. (a)–(c) Real orbitals at $B=0$. (e)–(g) The modulus square of the complex orbitals for a vanishingly small value $B=0.0001$ T. (d) The corresponding circular electron density for both cases. The choice of the remaining parameters is: $\hbar\omega_0=5$ meV and $m^*=0.067m_e$. Distances are in nanometers. The real orbitals are in 10^{-3} nm^{-1} and the orbital densities and total ED in 10^{-4} nm^{-2}. The arrows indicate the spin direction.

nants preserve the total spin, but for this value of R_W the lowest in energy UHF solution is one with broken circular symmetry. As will be seen below, broken rotational symmetry does not imply no space symmetry, but a lower point-group symmetry. Before proceeding with the study of the BS solution, however, it will be helpful to review the symmetry-adapted RHF solution first. This RHF solution can be obtained from the UHF equations (3) and (4) by using a circular electron density guess as the input of the first iteration. In the independent particle model, the $N=3$, $S_z=3/2$, and $B=0$ 2D case corresponds to a closed electronic shell with configuration $1s1p_+1p_-$ or $1s1p_x1p_y$ $(p_\pm\propto p_x\pm ip_y \propto re^{\pm i\theta})$, and thus the independent-particle-model ED is necessarily circular. We will confirm that the RHF solution

conforms indeed to the prediction of the independent particle model, and subsequently we will contrast the UHF solution to it.

The RHF solution for $R_W=10$ and $B=0$ has an energy of 92.217 meV; the corresponding orbitals are real and are displayed in the left column of Fig. 3. They are like the $1s$ [Fig. 3(a)], $1p_x$ [Fig. 3(b)], and $1p_y$ [Fig. 3(c)] orbitals of the independent particle model. The nodeless $1s$ orbital has a maximum at $r>0$ due to the large Coulomb repulsion; its energy is 44.526 meV. The energy of the two degenerate p_x and p_y orbitals is 50.489 meV. Notice that neither the p_x nor p_y orbital is rotationally symmetric; however, the total ED [Fig. 3(d)] has the expected circular symmetry. It is of interest to obtain the RHF solution for a very small external mag-
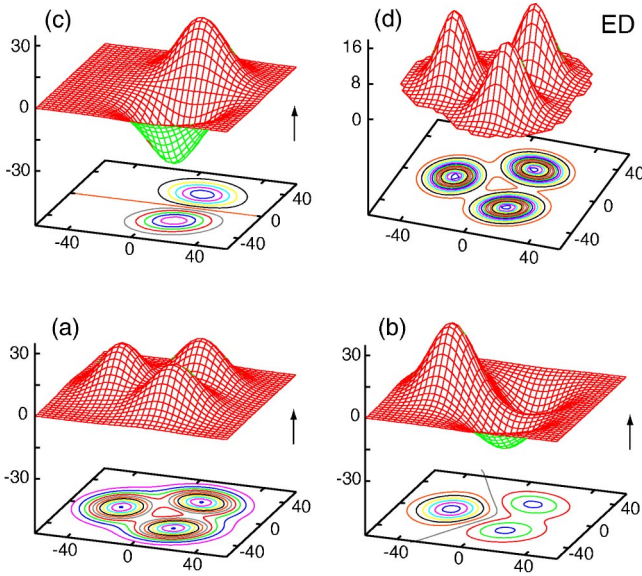
FIG. 4. The S-UHF case exhibiting breaking of the circular symmetry for $N=3$ and $S_z=3/2$ at $R_W=10$ and $B=0$. (a)–(c) Real orbitals. (d) The corresponding electron density. The choice of the remaining parameters is $\hbar\omega_0=5$ meV and $m^*=0.067m_e$. Distances are in nanometers. The real orbitals are in 10^{-3} nm^{-1} and the total ED in 10^{-4} nm^{-2}. The arrows indicate the spin direction.

netic field (i.e., in the limit $B\rightarrow 0$). In this case, the calculated total and orbital energies, as well as the total ED [Fig. 3(d)], remain unchanged. However, the two degenerate p orbitals are now complex [$p_\pm$; see Fig. 3(f) and Fig. 3(g)] and have good angular momenta $l=\pm 1$, and thus their modulus square is circularly symmetric.

We focus now on the sS-UHF solution for $N=3$ and $S_z=3/2$, and for the same choice of parameters as with the RHF case. The UHF total energy is 89.691 meV, and thus it is lower than the corresponding RHF one. In Fig. 4 we display the UHF symmetry-violating orbitals (a)–(c) whose energies are (a) 44.801 meV and (b) and (c) 46.546 meV; namely, the two orbitals (b) and (c) with the higher energies are again degenerate in energy. An inspection of Fig. 4 immediately reveals that these orbitals have retained some properties of the delocalized $1s$, $1p_x$, and $1p_y$ orbitals, familiar from the independent particle model and the RHF; that is, orbital (a) is nodeless, while each one of the orbitals (b) and (c) has a single nodal line. However, overall the BS orbitals (a)–(c) drastically differ from the orbitals of the independent particle model. In particular, they are associated with specific sites (within the QD) forming an equilateral triangle, and thus they can be described as having the structure of a linear combination of "atomic" (site) orbitals. Such LCAO MO's are familiar in natural molecules, and this analogy supports the term "electron (or Wigner) molecules" for characterizing the BS UHF solutions.

In the LCAO-MO approximation, one needs to solve a matrix eigenvalue equation determined by the overlaps S_{ij} ($i\neq j$) and the Hamiltonian matrix elements $\tilde{H}_{ij}$ and $\tilde{H}_{ii}$ between the atomic orbitals. A further simplified approximation,[48] the Hückel approximation (HüA), consists

in taking all $S_{ij}=0$, and all $\tilde{H}_{ij}=0$ unless the ith and jth atoms (sites) are adjacent. For our example this latter approximation is applicable, since the value $R_W=10$ is rather high. When using the notation $\epsilon=\tilde{H}_{11}=\tilde{H}_{22}=\tilde{H}_{33}$ and $-\beta=\tilde{H}_{12}=\tilde{H}_{13}=\tilde{H}_{23}<0$, the Hückel eigenvalue equation for the case of $N=3$ electrons on the vertices of an equilateral triangle is written as

$$\begin{pmatrix} \epsilon & -\beta & -\beta \\ -\beta & \epsilon & -\beta \\ -\beta & -\beta & \epsilon \end{pmatrix} \begin{pmatrix} f_1 \\ f_2 \\ f_3 \end{pmatrix} = E \begin{pmatrix} f_1 \\ f_2 \\ f_3 \end{pmatrix}, \qquad (13)$$

and the associated LCAO-MO's are $\psi_i=f_1^i\phi_1+f_2^i\phi_2+f_3^i\phi_3$, having E_i eigenvalues with $i=1,2,3$. The ϕ_j's are the original Gaussian-type atomic (site) orbitals.

From the eigenvalues and eigenvectors of Eq. (13), one finds the following three LCAO-MO's:

$$\psi_1=(\phi_1+\phi_2+\phi_3)/\sqrt{3} \qquad (14)$$

with energy $E_1=\epsilon-2\beta$,

$$\psi_2=(2\phi_1-\phi_2-\phi_3)/\sqrt{6} \qquad (15)$$

with energy $E_2=\epsilon+\beta$, and

$$\psi_3=(\phi_2-\phi_3)/\sqrt{2} \qquad (16)$$

with energy $E_3=E_2$. It is apparent that the structure of these three LCAO-MO's and the level diagram of their energies agree very well with the corresponding symmetry-broken UHF orbitals [displayed in Figs. 4(a)–4(c)] and their energies. (Using the HF values for E_1 and E_2, one finds $\epsilon\approx 45.961$ meV and $\beta\approx 0.585$ meV.) We notice here that such LCAO orbitals are familiar in organic chemistry and are associated with the theoretical description of carbocyclic systems and, in particular, the molecule C_3H_3 (cyclopropenyl, see, e.g., Ref. 33).

Naturally, since the orbitals (b) and (c) are degenerate in energy, they are not uniquely defined: any linear combination associated with a unitary 2×2 transformation will produce a pair of different, but equivalent (b') and (c') orbitals. The fact that the UHF orbitals in Fig. 4 have the specific highly symmetrized (see below) form given above is the result of an accidental choice of the initial electron density input in the HF iteration. We have checked that any such pair of (b') and (c') orbitals leaves the 2D total UHF electron density unchanged. This suggests that there is an underlying group theoretical structure that governs the BS UHF orbitals. The important point is not the uniqueness or not of the 2D sS-UHF orbitals, but the fact that they transform according to the irreducible representations of specific point groups, leaving both the sS-UHF determinant and the associated electron densities invariant. Given the importance of this observation, we proceed in the rest of this section with a group theoretical analysis of the BS sS-UHF orbitals for the $N=3$ and $S_z=3/2$ case.

The ED portrayed in Fig. 4(d) remains invariant under certain geometrical symmetry operations—namely, those of an unmarked, plane and equilateral triangle. They are (1) the

TABLE I. Character table for the cyclic group C_3 [$\varepsilon = \exp(2\pi i/3)$].

C_3	E	C_3	C_3^2
A	1	1	1
E'	1	ε	ε^*
E''	1	ε^*	ε

identity E, (2) the two rotations C_3 (rotation by $2\pi/3$) and C_3^2 (rotation by $4\pi/3$), and (3) the three reflections σ_v^I, σ_v^{II}, and σ_v^{III} through the three vertical planes, one passing through each vertex of the triangle. These symmetry operations for the unmarked equilateral triangle constitute the elements of the group C_{3v}.[33,49]

One of the main applications of group theory in chemistry is the determination of the eigenfunctions of the Schrödinger equation without actually solving the matrix equation (13). This is achieved by constructing the so-called *symmetry-adapted linear combinations* (SALC's) of AO's. A widely used tool for constructing SALC's is the projection operator

$$\hat{\mathcal{P}}^\mu = \frac{n_\mu}{|\mathcal{G}|} \sum_R \chi^\mu(R)\hat{R}, \qquad (17)$$

where $\hat{R}$ stands for any one of the symmetry operations of the molecule, and $\chi^\mu(R)$ are the characters of the μth irreducible representation of the set of $\hat{R}$'s. (The χ^μ's are tabulated in the socalled character tables.[33,49]) $|\mathcal{G}|$ denotes the order of the group and n_μ the dimension of the representation.

The task of finding the SALC's for a set of three $1s$-type AO's exhibiting the C_{3v} symmetry of an equilateral triangle can be simplified, since pure rotational symmetry by itself (the rotations C_3 and C_3^2, and not the reflections σ_v's through the vertical planes) is sufficient for their determination. Thus one needs to consider the simpler character table[50] of the cyclic group C_3 (see Table I).

From Table I, one sees that the set of the three $1s$ AO's situated at the vertices of an equilateral triangle spans the two irreducible representations A and E, the latter one consisting of two associated one-dimensional representations. To construct the SALC's, one simply applies the three projection operators $\hat{\mathcal{P}}^A$, $\hat{\mathcal{P}}^{E'}$, and $\hat{\mathcal{P}}^{E''}$ to one of the original AO's, let us say the ϕ_1,

$$\hat{\mathcal{P}}^A\phi_1 \approx (1)\hat{E}\phi_1 + (1)\hat{C}_3\phi_1 + (1)\hat{C}_3^2\phi_1$$

$$= (1)\phi_1 + (1)\phi_2 + (1)\phi_3 = \phi_1 + \phi_2 + \phi_3, \quad (18)$$

$$\hat{\mathcal{P}}^{E'}\phi_1 \approx (1)\hat{E}\phi_1 + (\varepsilon)\hat{C}_3\phi_1 + (\varepsilon^*)\hat{C}_3^2\phi_1$$

$$= \phi_1 + \varepsilon\phi_2 + \varepsilon^*\phi_3, \qquad (19)$$

$$\hat{\mathcal{P}}^{E''}\phi_1 \approx (1)\hat{E}\phi_1 + (\varepsilon^*)\hat{C}_3\phi_1 + (\varepsilon)\hat{C}_3^2\phi_1$$

$$= \phi_1 + \varepsilon^*\phi_2 + \varepsilon\phi_3. \qquad (20)$$

The A SALC in Eq. (18) has precisely the same form as the ψ_1 MO in Eq. (14), which was determined via a solution of the Hückel Eq. (13). The two E SALC's [Eq. (19) and Eq. (20)], however, are complex functions and do not coincide with the real ψ_2 and ψ_3 found above [Eq. (15) and Eq. (16)]. As we will see in Sec. IV, these complex SALC's agree with the BS UHF orbitals obtained in the case of an applied magnetic field $B \to 0$. On the other hand, a set of two real and orthogonal SALC's that spans the E representation can be derived fron Eq. (19) and Eq. (20) by simply adding and substracting the two complex ones. This procedure recovers immediately the real ψ_2 and ψ_3 discussed earlier.

We stress here that the UHF orbitals of Fig. 4 are *canonical* (see Sec. II A). As is well known from quantum chemistry,[26] in general the canonical spin orbitals will be spread out over the different sites (atoms) of a natural molecule and will form a basis for the irreducible representations of the symmetry group of the molecule. Once the canonical orbitals are available, there is an infinite number of *noncanonical* spin orbitals that span *reducible* representations of the symmetry group of the molecule and can be obtained via a unitary transformation of the canonical set. We remind the reader that noncanonical spin orbitals are solutions of a generalized HF equation involving off-diagonal elements E_{ij} in the matrix formed out of the HF orbital energies (see Sec. II A). Naturally, the unitary transformation leaves the UHF determinant and total energy invariant. In particular there is a unitary matrix that transforms the canonical spin orbitals to the fully localized AO's; i.e., for the $N=3$ and $S_z=3/2$ case, such a unitary matrix transforms the canonical ψ_i's ($i=1,2,3$) to the noncanonical AO's ϕ_i's.

Note that such noncanonical orbitals for $N=3$ were recently used[51] to formulate a non-self-consistent variant to the Pople-Nesbet HF equations listed in section II.A. This variant relied on the manifestation of spontaneous symmetry breaking that was discovered earlier via our self-consistent UHF results. Notice, however, that Ref. 51 obtained an incomplete wave function, since the companion step of restoration of the rotational symmetry was not considered (see Sec. VI below).

B. $S_z = 1/2$ partially spin polarized case

In Fig. 5, we display the sS-UHF symmetry-violating orbitals (a)–(c) for the case of a partially polarized QD at $R_W = 10$ and $B=0$ with two spin-up and one spin-down electrons ($N=3$ and $S_z=1/2$). The UHF orbital energies of these electrons are (a) 45.350 and (b) 46.515 meV for the spin-up orbitals and (c) 45.926 meV for the spin-down orbital. An inspection of Fig. 5 reveals that these orbitals have retained the nodal structure of the corresponding independent-particle-model orbitals in the familiar $1s^2 1p_x$ configuration; namely, (a) and (c) are nodeless, while (b) exhibits a single nodal line. Apart from this property, however, and in consonance with the $S_z=3/2$ case studied in a previous subsection, the BS UHF orbitals again differ drastically from the ones associated with the independent particle model; again they are associated with three sites within the QD arranged in an
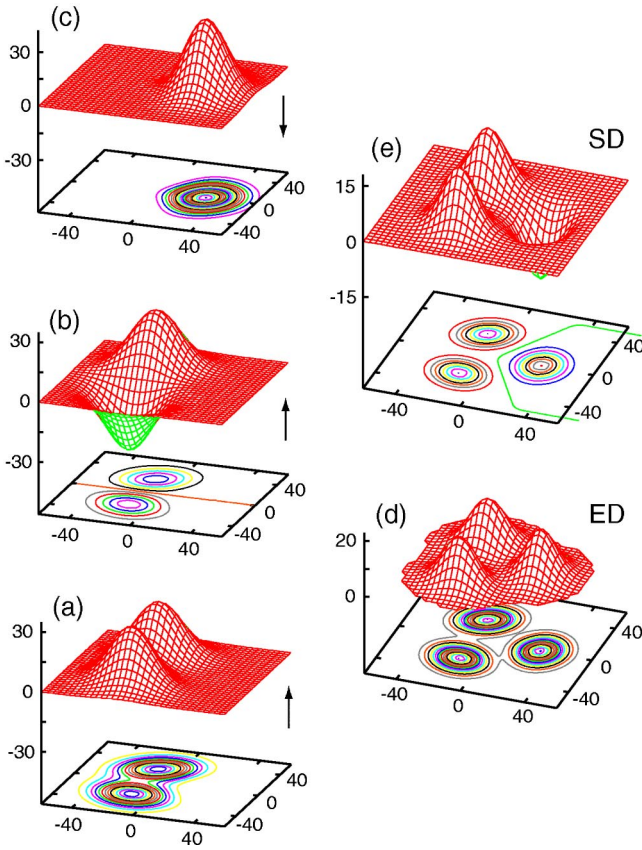
FIG. 5. The sS-UHF solution exhibiting breaking of the circular symmetry for $N=3$ and $S_z=1/2$ at $R_W=10$ and $B=0$. (a)–(b) Real orbitals for the two spin-up electrons. (c) Real orbital for the single spin-down electron. (d) Total electron density. (e) Spin density (difference of the spin-up minus the spin-down partial electron densities). The choice of the remaining parameters is $\hbar\omega_0=5$ meV and $m^*=0.067m_e$. Distances are in nanometers. The real orbitals are in 10^{-3} nm^{-1} and the densities (ED and SD) in 10^{-4} nm^{-2}. The arrows indicate the spin direction.

equilateral triangle. In contrast to the fully polarized case, however, there are no linear combinations of atomic orbitals involving all three vertices of the triangle. Indeed the single spin-down electron remains by itself as an unmodified AO, while only the two spin-up electrons combine to form LCAO MO's. This behavior here is a special case of a general property of the sS-UHF; i.e., only AO's associated with the same spin direction can in principle combine to form LCAO MO's. This property, however, does not extend to the generalized Hartree-Fock method,[31,52] which incorporates the additional unrestriction that the z projection (S_z) of the total spin is not preserved and it is not a good quantum number. (Notice that unlike the practice in this paper, Ref. 31 uses the term UHF for the generalized HF.)

TABLE II. Character table for the group $\{E, \sigma_v^I\}$.

	E	σ_v^I
A_2	1	-1
B_1	1	1

In the same spirit with the treatment of the fully polarized case in Sec. III A, and taking into consideration the decoupling of the two different spin directions in the sS-UHF, one can write a corresponding Hückel matrix equation for the $N=3$ and $S_z=1/2$ case as follows:

$$\begin{pmatrix} \epsilon & -\beta & 0 \\ -\beta & \epsilon & 0 \\ 0 & 0 & \epsilon \end{pmatrix} \begin{pmatrix} f_1 \\ f_2 \\ f_3 \end{pmatrix} = E \begin{pmatrix} f_1 \\ f_2 \\ f_3 \end{pmatrix}. \tag{21}$$

From the eigenvalues and eigenvectors of Eq. (21), one finds the following three LCAO-MO's: (a) $\psi_1=(\phi_1+\phi_2)/\sqrt{2}$ with energy $E_1=\epsilon-\beta$, (b) $\psi_2=(\phi_1-\phi_2)/\sqrt{2}$ with energy $E_2=\epsilon+\beta$, and (c) $\psi_3=\phi_3$ with energy $E_3=\epsilon$. The structure of these three LCAO-MO's agrees very well with the corresponding symmetry-violating UHF orbitals for the $N=3$ and $S_z=1/2$ case displayed in Figs. 5(a)–5(c). This agreement extends also to the level diagrams of the corresponding orbital energies. (Using the UHF values for E_1 and E_2, one finds $\beta=0.582$ meV and $\epsilon=45.932$ meV$\approx E_3$.)

Concerning the underlying symmetry-group structure of the UHF orbitals in Fig. 5, we observe that (unlike the fully polarized case) the two rotations—i.e., C_3 (rotation by $2\pi/3$) and C_3^2 (rotation by $4\pi/3$)—are not part of the symmetry operations of the relevant point group [due to the dissimilarity between spin-up and spin-down orbitals; this can be seen clearly through inspection of the spin density in Fig. 5(e)]. Because of the 2D character of the dot, the only symmetry operations for the $N=3$ and $S_z=1/2$ case are the identity E and a single reflection, σ_v^I, through the vertical plane passing through the spin-down electron. Such a group $\{E, \sigma_v^I\}$ is a subgroup of the familiar C_{2v} group associated with the 3D H_2O molecule (observe that the O atom corresponds to the spin-down electron and the two H atoms correspond to the two spin-up electrons). According to Ref. 33 (see p. 181), the representation Γ formed by the three original AO's can be reduced to irreducible A_2 and B_1 representations as $\Gamma=A_2+2B_1$. By applying projection operators [see Eq.(17)] to the ϕ_1 AO and using the character Table II, one finds the following two normalized SALC's:

$$\psi_{A_2}=(\phi_1-\phi_2)/\sqrt{2} \tag{22}$$

and

$$\psi_{B_1}=(\phi_1+\phi_2)/\sqrt{2}. \tag{23}$$

Naturally the second SALC of B_1 symmetry is

$$\psi'_{B_1}=\phi_3. \tag{24}$$

Once more, we stress the fact that the SALC's [Eqs. (22)–(24)] derived above via symmetry-group theory have the same structure as the canonical UHF orbitals displayed in Fig. 5. Observe further that in the generalized HF (as also in the case of the H_2O molecule and the allyl anion) the two SALC's of B_1 symmetry are allowed to couple, producing
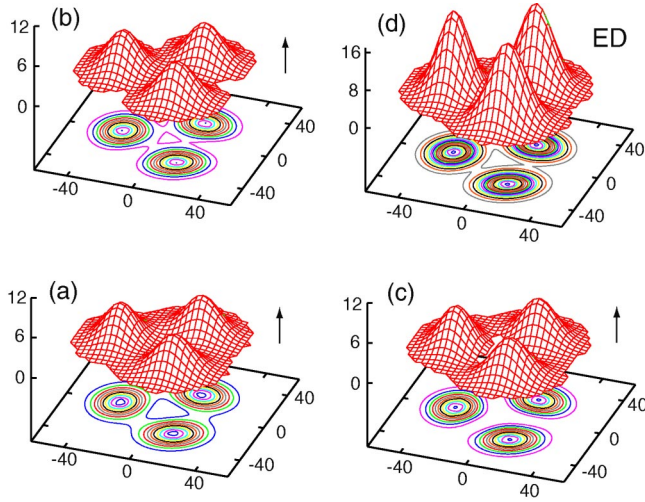
FIG. 6. The S-UHF solution exhibiting breaking of the circular symmetry for $N=3$ and $S_z=3/2$ at $R_W=10$ and $B=2$ T. (a)–(c) Orbitals (modulus square) for the three spin-up electrons. (d) Total electron density. The choice of the remaining parameters is $\hbar\omega_0 = 5$ meV, $m^*=0.067m_e$, and $g^*=-0.44$. Distances are in nanometers and the densities (orbital and ED) in 10^{-4} nm^{-2}. The arrows indicate the spin direction.

more complicated orbitals and energy level diagrams (see p. 1037 of Ref. 31 and p. 183 in Ref. 33)

IV. THREE ELECTRONS IN A FINITE MAGNETIC FIELD

A. $S_z=3/2$ fully polarized case

In this section, we study the case of three fully polarized electrons under a magnetic field B. Since for $B\neq0$ the BS UHF orbitals are necessarily complex functions, Fig. 6 displays the modulus square of these orbitals. The UHF total ED displayed in Fig. 6(d) and the modulus square of the orbitals exhibit an apparent C_{3v} symmetry as was the case at $B=0$ (Sec. III A). However, *the phases of the complex orbitals at $B\neq0$ contribute to a modification of the symmetry group*. This modification has been studied earlier for the case of infinite crystalline systems with periodic space lattices where the electrons occupy Bloch orbitals, and such studies have led to the consideration of two physically equivalent group structures: namely, the *ray groups*[53] and the *magnetic translation groups*.[54] In our case of a finite periodic crystallite, the corresponding magnetic rotation groups would be straightforward to consider. However, in order to appreciate the modifications introduced by the magnetic field, it will be simpler to modify the Hückel (tight-binding) Hamiltonian according to the Harper-Peierls prescription,[55,56] which accounts for the magnetic gauge transformation when moving from one crystalline site to another.

Thus according to Peierls and Harper, the proper atomic orbitals $\tilde{\phi}_j$'s for $B\neq0$ (centered at $\mathbf{R}_j$) are the real ϕ_j's multiplied by an appropriate phase as follows,

$$\tilde{\phi}_j(\mathbf{r};\mathbf{R}_j)=\phi_j(\mathbf{r};\mathbf{R}_j)e^{(ie/\hbar c)\mathbf{A}(\mathbf{R}_j)\cdot\mathbf{r}}. \tag{25}$$

Because of this position-dependent phase in the AO's, the hopping matrix elements $\tilde{H}_{ij}$ (see Sec. III A) are now complex, and the Hückel equation (13) for three electrons is modified as follows:

$$\begin{pmatrix} \epsilon & -\beta e^{i\Omega} & -\beta e^{-i\Omega} \\ -\beta e^{-i\Omega} & \epsilon & -\beta e^{i\Omega} \\ -\beta e^{i\Omega} & -\beta e^{-i\Omega} & \epsilon \end{pmatrix}\begin{pmatrix} f_1 \\ f_2 \\ f_3 \end{pmatrix}=E\begin{pmatrix} f_1 \\ f_2 \\ f_3 \end{pmatrix}, \tag{26}$$

where $\Omega\equiv\Omega_{ij}=(e/\hbar c)\mathbf{A}(\mathbf{R}_j-\mathbf{R}_i)\cdot\mathbf{R}_i$, $(i,j)=(1,2),(2,3),(3,1)$, with $\mathbf{R}_k$, $k=1,2,3$ being the positions of the vertices of the equilateral triangle. Notice that $\Omega=(2\pi\Phi)/(3\Phi_0)$, where Φ is the total magnetic flux through the equilateral triangle and $\Phi_0=hc/e$ is the unit flux.

From the eigenvectors of Eq. (26), one finds the following LCAO-MO's:

$$\psi_1\propto\tilde{\phi}_1+\tilde{\phi}_2+\tilde{\phi}_3, \tag{27}$$

$$\psi_2\propto e^{2\pi i/3}\tilde{\phi}_1+e^{-2\pi i/3}\tilde{\phi}_2+\tilde{\phi}_3, \tag{28}$$

$$\psi_3\propto e^{-2\pi i/3}\tilde{\phi}_1+e^{2\pi i/3}\tilde{\phi}_2+\tilde{\phi}_3, \tag{29}$$

with corresponding orbital energies

$$E_1=\epsilon-2\beta\cos\Omega, \tag{30}$$

$$E_2=\epsilon-2\beta\cos[(2\pi/3+\Omega)], \tag{31}$$

$$E_3=\epsilon-2\beta\cos[(2\pi/3-\Omega)]. \tag{32}$$

Substituting the specific value for Ω given above, one can write the eigenvalues (30)–(32) in a more symmetric compact form

$$E_j=\epsilon-2\beta\cos\left[\frac{2\pi}{3}\left(j+\frac{\Phi}{\Phi_0}\right)\right], \quad j=1,2,3. \tag{33}$$

Since the original AO's do not practically overlap for $R_W=10$, the phases in front of the ϕ_i's in Eqs. (27)–(29) do not contribute substantially to the modulus square of the orbitals. As a result, for all values of B, all three orbitals exhibit similar orbital densities that are approximately equal to $\phi_1^2+\phi_2^2+\phi_3^2$. Observe that this agrees very well with the behavior of the canonical UHF orbitals (modulus square) at $B=2$ T displayed in Fig. 6. At zero magnetic field $B=0$, the LCAO-MO's in Eqs. (27)–(29) reduce to the specific form given earlier in Eqs. (18)–(20) of Sec. III A. We stress here that in Sec. III A these LCAO-MO's were derived from arguments based exclusively on the group theoretical structure of the C_{3v} symmetry group.

Naturally, when $\Omega=0$, the orbital energies in Eq. (33) reduce to the corresponding $B=0$ result derived in Sec. III A: namely, $E_1=\epsilon-2\beta$ and $E_2=E_3=\epsilon+\beta$. Notice, however, that for arbitrary values of B, the degeneracy between E_2 and E_3 is lifted. In addition, the three energies E_1, E_2, and E_3 in Eq. (33) exhibit prominent Aharonov-Bohm (AB) oscillations. It is interesting to compare this behavior to the
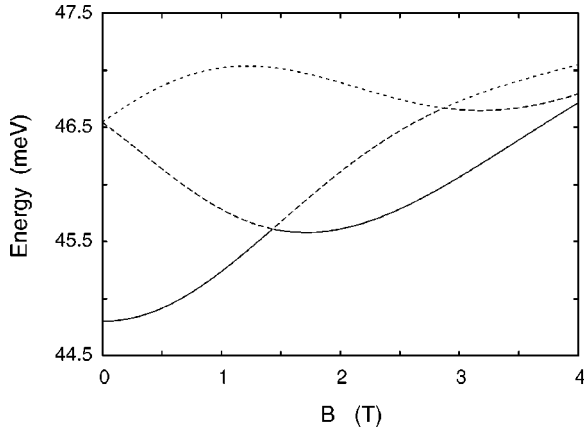
FIG. 7. The S-UHF orbital energies (in meV) for $N=3$, $S_z=3/2$, and $R_W=10$ as a function of the magnetic field B (in tesla), exhibiting a prominent Aharonov-Bohm oscillation. The choice of the remaining parameters is $\hbar\omega_0=5$ meV, $m^*=0.067m_e$, and $g^*=-0.44$.

FIG. 8. The sS-UHF solution exhibiting breaking of the circular symmetry for $N=3$, $S_z=1/2$ at $R_W=10$ and $B=2$ T. (a)–(b) Orbitals (modulus square) for the two spin-up electrons. (c) Orbital (modulus square) for the spin-down electron. (d) Total electron density. The choice of the remaining parameters is $\hbar\omega_0=5$ meV, $m^*=0.067m_e$, and $g^*=-0.44$. Distances are in nanometers and the densities (orbital and ED) in 10^{-4} nm^{-2}. The arrows indicate the spin direction.

behavior of the calculated canonical UHF orbital energies for $R_W=10$. These UHF orbital energies as a function of B are displayed in Fig. 7. An inspection of Fig. 7 reveals that the UHF orbital energies do exhibit (as expected) an Aharonov-Bohm oscillation as a function of B. However, these oscillations are more complicated from what can be simply anticipated from the analytic formulas in Eq. (33). Namely, the amplitude of the UHF AB oscillations decreases as B increases. This behavior is due to a decrease in the hopping parameter β, which results from the spatial shrinkage of the Gaussian-type UHF orbitals as a function of B. Eventually, for $B\to\infty$, all three energies are degenerate. We notice that complete degeneracy of all UHF orbitals for any N appears also in the $B=0$, $R_W\to\infty$ limit.

The electronic structure of the UHF fully polarized three-electron molecule in a magnetic field, which was discussed above and which exhibits Aharonov-Bohm oscillations, does not have an analog in the realm of natural molecules. However, apart from the B dependence of β, it agrees in a remarkable way with the "noninteracting spectra" of the artificial molecules that can be formed out of 1D ring arrays of single QD's.[57]

B. $S_z=1/2$ partially polarized case

Figure 8 displays the BS UHF orbitals (modulus square) and the total ED for the partially polarized $N=3$, $S_z=1/2$ case in a magnetic field $B=2$ T. As with the $B=0$ case (Sec. III B), the spin-down orbital is decoupled from the two spin-up ones. As a result the corresponding Hückel matrix equation is of the form

$$\begin{pmatrix} \epsilon & -\beta e^{i\Omega} & 0 \\ -\beta e^{-i\Omega} & \epsilon & 0 \\ 0 & 0 & \epsilon' \end{pmatrix} \begin{pmatrix} f_1 \\ f_2 \\ f_3 \end{pmatrix} = E \begin{pmatrix} f_1 \\ f_2 \\ f_3 \end{pmatrix}, \quad (34)$$

where in general $\epsilon'\neq\epsilon$ due to the energy difference between the two spin directions introduced by the Zeeman term. From the solutions of Eq. (34), one finds the following LCAO-
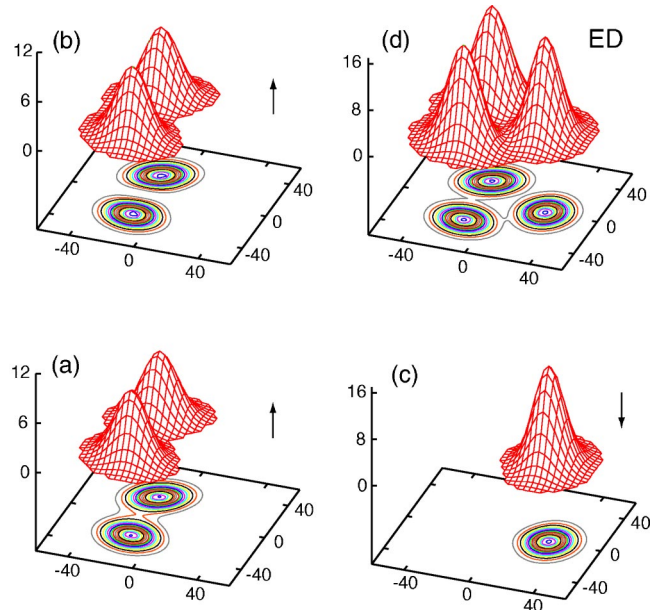
MO's: (a) $\psi_1=(e^{i\Omega}\tilde{\phi}_1+\tilde{\phi}_2)/\sqrt{2}$ with energy $E_1=\epsilon-\beta$, (b) $\psi_2=(e^{i\Omega}\tilde{\phi}_1-\tilde{\phi}_2)/\sqrt{2}$ with energy $E_2=\epsilon+\beta$, and (c) $\psi_3=\tilde{\phi}_3$ with $E_3=\epsilon'$. The total electron density constructed out of these LCAO-MO's is again of the form $\phi_1^2+\phi_2^2+\phi_3^2$ (compare with Sec. IV A). The corresponding UHF orbitals (modulus square) and ED displayed in Fig. 8 are obviously conforming to these forms.

Concerning the Hückel orbital energies E_j, $j=1,2,3$, we note that they do not depend on the magnetic field B through Ω. As a result, unlike the previous case of the fully polarized electrons, AB oscillations should not develop in the UHF orbital energies. To check this prediction, we dispaly in Fig. 9 the UHF orbital energies as a function of B. In contrast to Fig. 7, AB oscillations are absent in Fig. 9, a behavior which apparently relates to the fact that no UHF orbital covers the area of the equilateral triangle (the single spin-down orbital does not couple to the two spin-up ones, which lie on a straight line).

V. SIX ELECTRONS AT ZERO MAGNETIC FIELD

We discuss now the case of six fully polarized electrons in zero magnetic field. The corresponding total S-UHF electron density for $R_W=15$ ($\kappa=1.2730$) is displayed in Fig. 10(a) (bottom frame). Unlike the case of smaller numbers of particles with $N\leq5$, a system of six electrons is the smallest that forms a Wigner molecule with a two-ring arrangement. Such a ring arrangement is denoted by (1,5) to distinguish it from a single-ring arrangement (0,N).
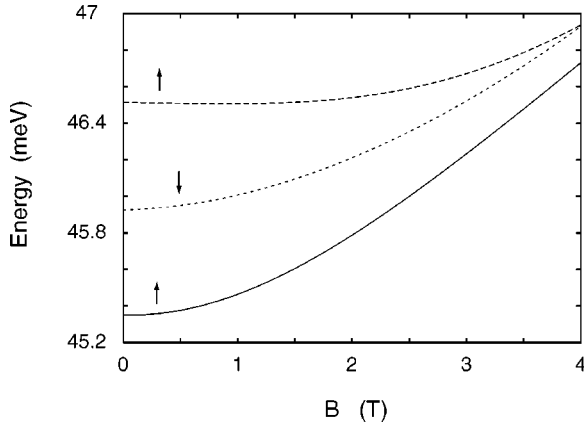
FIG. 9. The sS-UHF orbital energies (in meV) for $N=3$, $S_z = 1/2$, and $R_W = 10$ as a function of the magnetic field B (in tesla). No AB oscillations are present. The choice of the remaining parameters is $\hbar\omega_0 = 5$ meV, $m^* = 0.067 m_e$, and $g^* = -0.44$. The arrows indicate the spin direction.

Naturally, single-ring molecular arrangements $(0,N)$ are familiar from the quantum chemistry of carbocyclic systems (Ref. 33; see also Secs. III and IV). The more complicated $(1,5)$ arrangement, however, is a molecular structure unknown to traditional chemistry. Nevertheless, contact to organic chemistry can be retained by observing that the $(0,5)$ outer ring has a group symmetry similar to the cyclic hydrocarbon C_5H_5. As a result, and in direct analogy with the C_5H_5 molecule (see p. 152 in Ref. 33), the SALC's of the $(0,5)$ arrangement are as follows:

$$\psi(A) = \frac{1}{\sqrt{5}}(\phi_1 + \phi_2 + \phi_3 + \phi_4 + \phi_5), \tag{35}$$

$$\psi(E_1 a) = \sqrt{\frac{2}{5}}(\phi_1 + \phi_2 \cos\theta + \phi_3 \cos 2\theta + \phi_4 \cos 2\theta + \phi_5 \cos\theta), \tag{36}$$

$$\psi(E_1 b) = \sqrt{\frac{2}{5}}(\phi_2 \sin\theta + \phi_3 \sin 2\theta - \phi_4 \sin 2\theta - \phi_5 \sin\theta), \tag{37}$$

$$\psi(E_2 a) = \sqrt{\frac{2}{5}}(\phi_1 + \phi_2 \cos 2\theta + \phi_3 \cos\theta + \phi_4 \cos\theta + \phi_5 \cos 2\theta), \tag{38}$$

$$\psi(E_2 b) = \sqrt{\frac{2}{5}}(\phi_2 \sin 2\theta - \phi_3 \sin\theta + \phi_4 \sin\theta - \phi_5 \sin 2\theta), \tag{39}$$

where $\theta = 2\pi/5$. The corresponding orbital energies are $\epsilon - 2\beta$ for the single orbital of A symmetry, $\epsilon - (2\cos\theta)\beta$ for the two degenerate orbitals of E_1 symmetry, and $\epsilon - (2\cos 2\theta)\beta$ for the remaining two degenerate orbitals of E_2 symmetry.
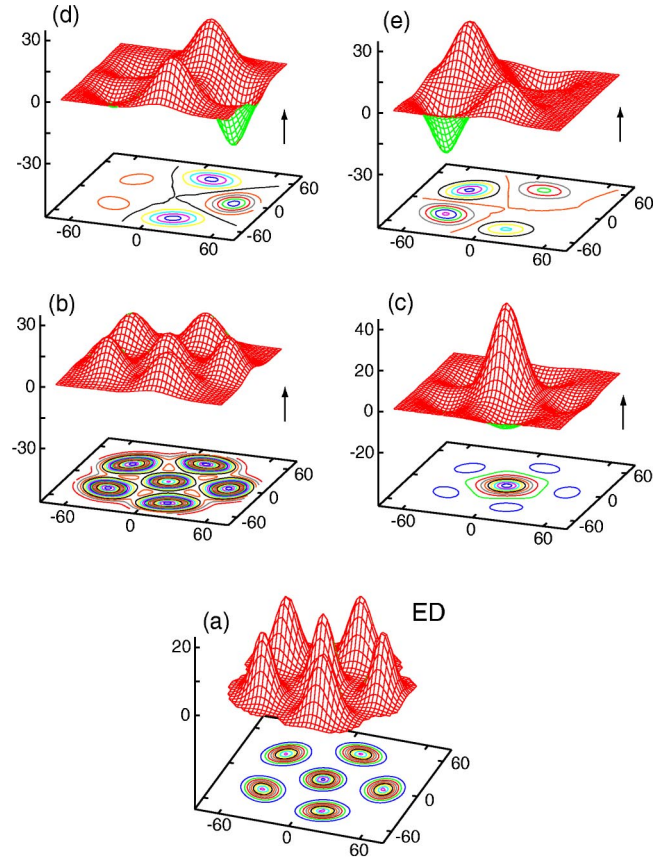

FIG. 10. The canonical S-UHF real orbitals for $N=6$ and $S_z = 3$ and for $R_W = 15$ and $B = 0$. (a) The total electron density. (b), (c) Middle row: the two orbitals of A symmetry. (d), (e) Top row: the two degenerate orbitals of E_2 symmetry. The choice of the remaining parameters is $\hbar\omega_0 = 5$ meV and $m^* = 0.067 m_e$. Distances are in nanometers. The real orbitals are in 10^{-3} nm^{-1} and the electron density in 10^{-4} nm^{-2}. The arrows indicate the spin direction.

Returning back to the case of the $(1,5)$ ring arrangement, we notice that the sixth AO, ϕ_6, at the center is of A symmetry, and thus it can only couple to a MO of the $(0,5)$ ring with the same symmetry; namely, the orbital $\psi(A)$ in Eq. (35). As a result, both $(0,5)$ and the $(1,5)$ ring arrangements share the same four MO's of E_1 and E_2 symmetry.

The coupling matrix element between the ϕ_6 and $\psi(A)$ orbitals is given by

$$\int \phi_6 \tilde{H} \psi(A) d\mathbf{r} = \frac{1}{\sqrt{5}} \sum_{k=1}^{5} \int \phi_6 \tilde{H} \phi_k d\mathbf{r} = -\sqrt{5}\,\delta. \tag{40}$$

To find the MO's of the $(1,5)$ ring with A symmetry, we need to solve the 2×2 matrix equation

$$\begin{pmatrix} \epsilon - 2\beta & -\sqrt{5}\,\delta \\ -\sqrt{5}\,\delta & \tilde{\epsilon} \end{pmatrix} \begin{pmatrix} g_1 \\ g_2 \end{pmatrix} = E \begin{pmatrix} g_1 \\ g_2 \end{pmatrix}. \tag{41}$$

We note that, due to the different coordination and distances, the quantities δ and $\tilde{\epsilon}$ associated with the central AO

are different from the corresponding quantities β and ϵ associated with the AO's of the outer ring.

Using the notation

$$Q = \sqrt{20\delta^2 + (\widetilde{\epsilon} - \epsilon + 2\beta)^2}, \qquad (42)$$

the two solutions of the matrix equation (41) have energies $(\widetilde{\epsilon} + \epsilon - 2\beta \mp Q)/2$ and eigenvectors (unnormalized) $\{\widetilde{\epsilon} - \epsilon + 2\beta \pm Q, \sqrt{20}\delta\}$, respectively. Accordingly, one MO of the (1,5) ring is constructed by adding and the other by subtracting a fraction of the $\psi(A)$ orbital from the central AO. This behavior agrees very well with the two S-UHF orbitals displayed in the middle row of Fig. 10 [(b) and (c)].

Concerning the S-UHF orbitals displayed in the top row of Fig. 10 [(d) and (e)], we notice that they are degenerate in energy and that they agree very well with the two MO's of E_2 symmetry. Indeed the S-UHF orbital in Fig. 10(d) exhibits five total humps, three of them positive and the other two negative, in remarkable agreement (apart from an overall sign) with the MO in Eq. (38) (note that $\cos\theta = 0.3090 > 0$ and $\cos 2\theta = -0.8090 < 0$). In particular, counterclockwise, the polarities of the humps in Fig. 10(d) are $(-,+,-,-,+)$, differing only by an overall sign from the corresponding polarities of the MO in Eq. (38). Even more impressive is the fact that there is quantitative agreement regarding the absolute heights of the humps in these two orbitals (see the values of $\cos\theta$ and $\cos 2\theta$ listed above). The other S-UHF orbital in Fig. 10(e) exhibits a total of four humps, two of them positive and the other two negative, and having an alternating $(+,-,+,-)$ arrangement. This is again in remarkable agreement with the second MO of E_2 symmetry in Eq. (39), since $\sin\theta > 0$ and $\sin 2\theta > 0$. Additionally, we note that the agreement between the UHF orbital in Fig. 10(e) and the MO in Eq. (39) extends further to the absolute heights of the humps, since $\sin\theta = 0.9511 > 0.5878 = \sin 2\theta$.

Finally, there are two other degenerate UHF orbitals that are not displayed in Fig. 10. They are not identical to the $\psi(E_1 a)$ and $\psi(E_1 b)$ SALC's in Eqs. (36) and (37), but we have checked that they span the E_1 irreducible representation.

VI. RESTORATION OF CIRCULAR SYMMETRY AND EXACT SPECTRA

A. Group structure and sequences of magic angular momenta

In the previous sections, we demonstrated that the BS UHF determinants and orbitals describe indeed 2D electronic molecular stuctures (Wigner molecules) in close analogy with the case of natural 3D molecules. However, the study of the WM's at the UHF level restricts their description to the *intrinsic* (nonrotating) frame of reference. Motivated by the case of natural atoms, one can take a subsequent step and address the properties of *collectively* rotating WM's in the laboratory frame of reference. As is well known, for natural atoms, this step is achieved by writing the total wave function of the molecule as the product of the electronic and ionic partial wave functions. In the case of the purely electronic WM's, however, such a product wave function requires the assumption of complete decoupling between intrinsic and

collective degrees of freedom, an assumption that might be justifiable in limiting cases only.

As we demonstrated earlier,[15–17] in the framework of the BS UHF solutions this companion step can be performed by using the post-Hartree-Fock method of *restoration of broken symmetries*[25] (RBS) via projection techniques (PT's). Examples demonstrating the RBS method have been presented by us in two cases: (I) the ground state (with angular momentum $I = 0$) of two interacting electrons in a parabolic quantum dot in the absence of a magnetic field[15] and (II) the yrast rotational band (see Sec. I C and precise definition in Ref. 58) of a system of N interacting electrons in high magnetic fields[16,17] (fractional-quantum-Hall regime). In both cases, we showed that the RBS method (as adapted to the case of 2D BS UHF solutions) yields correlated (multideterminantal) many-body wave functions that approximate very well the corresponding exact solutions.[58] In particular, in the latter case, our use[16,17] of the RBS method yielded analytic expressions for the correlated wave functions that offer a better description of the N-electron problem in high B compared to the Jastrow-Laughlin[5] expression.

In this section, we will not proceed any further with explicit numerical or analytic derivations of additional RBS wave functions. Instead, we will use the RBS approach to illustrate through a couple of concrete examples how certain universal properties of the exact solutions—i.e., the appearance of magic angular momenta in the exact rotational spectra[35–40]—relate to the symmetry broken UHF solutions. Indeed, *we will demonstrate that the magic angular momenta are a direct consequence of the symmetry breaking at the UHF level and that they are determined fully by the molecular symmetries of the UHF determinant.*[59]

As an illustrative example, we have chosen the relatively simple, but nontrivial, case of $N = 3$ electrons. For $B = 0$, both the $S_z = 1/2$ and $S_z = 3/2$ polarizations can be considered. We start with the $S_z = 1/2$ polarization, whose BS UHF solution (let us denote it by $|\downarrow\uparrow\uparrow\rangle$) was presented in Sec. III B and which exhibits a breaking of the total spin symmetry in addition to the rotational symmetry. We first proceed with the restoration of the total spin by noticing that $|\downarrow\uparrow\uparrow\rangle$ has a point-group symmetry lower (see Sec. III B) than the C_{3v} symmetry of an equilateral triangle. The C_{3v} symmetry, however, can be readily restored by applying the projection operator (17) to $|\downarrow\uparrow\uparrow\rangle$ and by using the character table of the cyclic C_3 group (see Table I). Then for the intrinsic part of the many-body wave function, one finds two different three-determinantal combinations: namely,

$$\Phi_{intr}^{E'}(\gamma_0) = |\downarrow\uparrow\uparrow\rangle + e^{2\pi i/3}|\uparrow\downarrow\uparrow\rangle + e^{-2\pi i/3}|\uparrow\uparrow\downarrow\rangle \quad (43)$$

and

$$\Phi_{intr}^{E''}(\gamma_0) = |\downarrow\uparrow\uparrow\rangle + e^{-2\pi i/3}|\uparrow\downarrow\uparrow\rangle + e^{2\pi i/3}|\uparrow\uparrow\downarrow\rangle, \quad (44)$$

where $\gamma_0 = 0$ denotes the azimuthal angle of the vertex associated with the original spin-down orbital in $|\downarrow\uparrow\uparrow\rangle$. We note

that the intrinsic wave functions $\Phi_{\text{intr}}^{E'}$ and $\Phi_{\text{intr}}^{E''}$ are eigenstates of the square of the total spin operator $\hat{\mathbf{S}}^2$ ($\hat{\mathbf{S}} = \Sigma_{i=1}^3 \hat{\mathbf{s}}_i$) with quantum number $s = 1/2$. This can be verified directly by applying $\hat{\mathbf{S}}^2$ to them.[60]

To restore the circular symmetry in the case of a $(0,N)$ ring arrangement, one applies the projection operator[15,25]

$$2\pi\mathcal{P}_I \equiv \int_0^{2\pi} d\gamma \exp[-i\gamma(\hat{L}-I)], \qquad (45)$$

where $\hat{L} = \Sigma_{j=1}^N \hat{l}_j$ is the operator for the total angular momentum. Notice that the operator $\mathcal{P}_I$ is a direct generalization of the projection operator (17) to the case of the continuous cyclic group C_∞ [the phases $\exp(i\gamma I)$ are the characters of C_∞].

The RBS-projected wave function Ψ_{RBS} (having both good total spin and angular momentum quantum numbers) is of the form

$$2\pi\Psi_{\text{RBS}} = \int_0^{2\pi} d\gamma \Phi_{\text{intr}}^E(\gamma)e^{i\gamma I}, \qquad (46)$$

where now the intrinsic wave function [given by Eq. (43) or Eq. (44)] has an arbitrary azimuthal orientation γ. We note that, unlike the phenomenological Eckardt-frame model[39,61] where only a single product term is involved, the RBS wave function in Eq. (46) is an average over all azimuthal directions of an infinite set of product terms. These terms are formed by multiplying the UHF intrinsic part $\Phi_{\text{intr}}^E(\gamma)$ by the external rotational wave function $\exp(i\gamma I)$ (the latter is properly characterized as "external," since it is an eigenfunction of the total angular momentum $\hat{L}$ and depends exclusively on the azimuthal coordinate γ).

The operator $\hat{R}(2\pi/3) \equiv \exp(-i2\pi\hat{L}/3)$ can be applied to Ψ_{RBS} in two different ways: namely, either to the intrinsic part Φ_{intr}^E or the external part $\exp(i\gamma I)$. Using Eq. (43) and the property $\hat{R}(2\pi/3)\Phi_{\text{intr}}^{E'} = \exp(-2\pi i/3)\Phi_{\text{intr}}^{E'}$, one finds

$$\hat{R}(2\pi/3)\Psi_{\text{RBS}} = \exp(-2\pi i/3)\Psi_{\text{RBS}}, \qquad (47)$$

from the first alternative, and

$$\hat{R}(2\pi/3)\Psi_{\text{RBS}} = \exp(-2\pi I i/3)\Psi_{\text{RBS}}, \qquad (48)$$

from the second alternative. Now if $\Psi_{\text{RBS}} \neq 0$, the only way that Eqs. (47) and (48) can be simultaneously true is if the condition $\exp[2\pi(I-1)i/3] = 1$ is fulfilled. This leads to a first sequence of magic angular momenta associated with total spin $s = 1/2$: i.e.,

$$I = 3k+1, \ k = 0, \pm 1, \pm 2, \pm 3, \dots. \qquad (49)$$

Using Eq. (44) for the intrinsic wave function and following similar steps, one can derive a second sequence of magic angular momenta associated with good total spin $s = 1/2$: i.e.,

$$I = 3k-1, \ k = 0, \pm 1, \pm 2, \pm 3, \dots. \qquad (50)$$

In the fully polarized case, the UHF determinant was described in Sec. III A. This UHF determinant, which we denote as $|\uparrow\uparrow\uparrow\rangle$, is already an eigenstate of $\hat{\mathbf{S}}^2$ with quantum number $s = 3/2$. Thus only the rotational symmetry needs to be restored; that is, the intrinsic wave function is simply $\Phi_{\text{intr}}^A(\gamma_0) = |\uparrow\uparrow\uparrow\rangle$. Since $\hat{R}(2\pi/3)\Phi_{\text{intr}}^A = \Phi_{\text{intr}}^A$, the condition for the allowed angular momenta is $\exp[-2\pi I i/3] = 1$, which yields the following magic angular momenta:

$$I = 3k, \ k = 0, \pm 1, \pm 2, \pm 3, \dots. \qquad (51)$$

We note that in high magnetic fields only the fully polarized case is relevant and that only angular momenta with $k > 0$ enter in Eq. (51) (see Ref. 16). In this case, in the thermodynamic limit, the partial sequence with $k = 2q+1$, $q = 0,1,2,3,\dots$, is directly related to the odd filling factors $\nu = 1/(2q+1)$ of the fractional quantum Hall effect [via the relation $\nu = N(N-1)/(2I)$]. This suggests that the observed hierarchy of fractional filling factors in the quantum Hall effect may be viewed as a signature originating from the point group symmetries of the intrinsic wave function Φ_{intr}, and thus it is a manifestation of symmetry breaking at the UHF mean-field level.

B. Quantitative description of the yrast band

The usefulness of the RBS wave functions [Eq. (46)] is not limited to deriving universal properties of the exact spectra, like the sequences of magic angular momenta [see Sec. VI A]. As we demonstrated in earlier publications, in the regime of strong correlations, the RBS wave functions approximate very well the corresponding exact many-body wave functions.

Indeed, in Ref. 15 we offered (as a function of R_W) a systematic comparison between the RBS and exact ground-state ($I = 0$) energies at $B = 0$ for $N = 2$ electrons in a parabolic QD. For $R_W = 19.09$, we found that the relative error was approximately 0.7%. Furthermore, in Ref. 16, for the case of high B, we derived *analytic* RBS wave functions, named "REM wave functions." As we showed[16] explicitly for the case of $N = 6$ electrons, the radial electron densities associated with the REM functions accurately reproduce the ones extracted from exact-diagonalization calculations.

In this subsection, we offer additional examples pertaining to the ability of the RBS wave functions to reproduce the exact yrast spectra of parabolic QD's. In particular, Table III lists the REM and exact yrast energies in the range of magic angular momenta $70 \leq I \leq 130$ for $N = 6$ electrons in high B. Details concerning the REM wave functions and the exact-diagonalization method in the lowest Landau level are given in Ref. 17, and they will not be repeated here.

The RBS and exact yrast spectra ($0 \leq I \leq 6$) for the case of $N = 2$ electrons at $B = 0$ and $R_W = 19.09$ are given in Table IV. Details concerning their calculation are given in Ref. 15 and in the Appendix (where we present the final formula for calculating RBS energies for both even and odd angular momenta).

We note that the relative errors in both Table III and Table IV are small (smaller than 1% in the majority of cases).

TABLE III. Case of $N=6$ electrons in high magnetic field B: total interaction energies in the lowest Landau level of REM and exact-diagonalization wave functions for various magic angular momenta I of the yrast band. The REM functions are analytically specified RBS wave functions derived in Ref. 16. The percentages within parentheses indicate relative errors. Energies in units of $e^2/\kappa l_B$, where κ is the dielectric constant and $l_B = \sqrt{\hbar c/eB}$ is the magnetic length. For details concerning the exact-diagonalization method and the REM wave functions, see Ref. 17. For additional values of I, see Ref. 17.

I	REM	Exact
70	2.3019 (0.85%)	2.2824
80	2.1455 (0.71%)	2.1304
90	2.0174 (0.60%)	2.0053
100	1.9098 (0.51%)	1.9001
110	1.8179 (0.45%)	1.8098
120	1.7382 (0.40%)	1.7312
130	1.6681 (0.36%)	1.6621

VII. SUMMARY

In this paper, we have introduced a group theoretical analysis of broken-symmetry UHF orbitals and total electron densities in the case of single 2D semiconductor QD's. This analysis provided further support for our earlier interpretation[9,10,14,15] concerning the spontaneous formation of collectively rotating electron (or Wigner) molecules. Indeed the group theoretical analysis enabled us to unveil further deeper analogies between the electronic structure of the Wigner molecules and that of the natural 3D molecules. In particular these deeper analogies are the following: (I) The breaking of rotational symmetry results in canonical UHF orbitals that are associated with the eigenvectors of a molecular-type Hückel Hamiltonian with sites at positions specified by the equilibrium configuration of the classical N-electron problem. (II) The broken-symmetry canonical UHF orbitals transform according to the irreducible repre-

TABLE IV. Case of $N=2$ electrons in a parabolic QD at $B=0$: total energies of RBS and exact wave functions for various magic angular momenta I of the yrast band. The percentages within parentheses indicate relative errors. The choice of remaining parameters is $\hbar\omega_0 = 5$ meV, $\kappa=1$ ($R_W = 19.09$), and $m^* = 0.067 m_e$. Energies in units of meV. For details concerning the method for finding exact solutions to the two-electron problem, see Ref. 14. For details concerning the calculation of the RBS yrast spectrum, see Ref. 15 and the Appendix.

I	RBS	Exact
0	52.224 (0.75%)	51.831
1	52.696 (0.77%)	52.292
2	54.086 (0.88%)	53.615
3	56.240 (1.04%)	55.654
4	59.065 (1.39%)	58.255
5	62.065 (1.27%)	61.285
6	63.911 (1.13%)	64.642

sentations of the point group specified by the discrete symmetries of this classical molecular configuration. (III) The WM's formed out of the broken-symmetry UHF solutions can rotate, and the restoration of the total-spin and rotational symmetries results (in addition to the ground state) in states defining the lowest rotational bands (i.e., yrast bands) of the WM's. (IV) The breaking of the circular symmetry results in lowering of the symmetry. This is expressed by the discrete point-group symmetry of the UHF wave function, and it underlies the appearance of sequences of magic angular momenta (familiar from exact-diagonalization studies) in the excitation spectra of single QD's.

Since exact-diagonalization methods are typically restricted to small sizes with $N \leq 10$, the two-step method of breakage and subsequent restoration of symmetries offers a promising new venue for accurately describing larger 2D electronic systems. A concrete example of the potential of this approach is provided by Ref. 16, where our use of the the symmetry-breaking and symmetry-restoration method yielded analytic expressions for correlated wave functions that offer a better description of the N-electron problem in high magnetic fields compared to the Jastrow-Laughlin[5] expression.

Furthermore, the group theoretical analysis strongly suggests an interesting simplified variant approach for carrying out the first step of symmetry breaking. This variant rests on the observation that, in all cases of WM's, the broken-symmetry UHF orbitals are generic linear combinations of Gaussian-type functions [with a proper phase for $B \neq 0$; see Eq. (25)] specified simply by their width σ and positions $\mathbf{R}_j$'s from the center of the QD. The linear combinations can be fully specified from the group theoretical analysis of the appropriate classical equilibrium configurations,[11] and a determinant of the corresponding LCAO-MO's can readily be written down. Then a simple variational calculation of the minimum total energy of this determinant will yield the parameters σ and $\mathbf{R}_j$'s without the need to carry out the self-consistent UHF iterations. This simplified approach could treat even larger sizes without major loss of accuracy. Added accuracy can then be obtained through the subsequent step of restoration of the broken symmetries.

ACKNOWLEDGMENTS

APPENDIX

For the case of $N=2$ electrons in a parabolic QD at $B=0$, we reported in Ref. 15 the RBS formulas for calculating energies of yrast-band states with *even* angular momenta I. These formulas [see Eqs. (11)–(13) in Ref. 15] were generated via a projection of the ''singlet'' UHF determinant. The corresponding RBS formulas for *odd* values of I are generated via a projection of the triplet UHF state.

In this appendix, we present the formulas covering both even and odd angular momenta. They are

$$E_{\mathrm{RBS}}(I) = \int_0^{2\pi} h(\gamma) e^{i\gamma I} d\gamma \Big/ \int_0^{2\pi} n(\gamma) e^{i\gamma I} d\gamma, \quad \text{(A1)}$$

with

$$h(\gamma) = H_{us}S_{vt} \pm H_{ut}S_{vs} + H_{vt}S_{us} \pm H_{vs}S_{ut} + V_{uvst} \pm V_{uvts}, \quad \text{(A2)}$$

and

$$n(\gamma) = S_{us}S_{vt} \pm S_{ut}S_{vs}, \quad \text{(A3)}$$

where the upper signs apply in the case of even I's and the lower signs in the case of odd I's. Here $s(\mathbf{r})$ and $t(\mathbf{r})$ are the initial $u(\mathbf{r})$ and $v(\mathbf{r})$ broken-symmetry UHF orbitals rotated by an angle γ, respectively. V_{uvst} and V_{uvts} are two-body matrix elements of the Coulomb repulsion, and S_{us}, etc., are the overlap intergrals.

---

[1] M.A. Kastner, Phys. Today **46** (1), 24 (1993).

[2] R.C. Ashoori, Nature (London) **379**, 413 (1996).

[3] S. Tarucha, D.G. Austing, T. Honda, R.J. van der Hage, and L.P. Kouwenhoven, Phys. Rev. Lett. **77**, 3613 (1996).

[4] L. P. Kouwenhoven, C. M. Marcus, P. L. McEuen, S. Tarucha, R. M. Westervelt, and N. S. Wingreen, Vol. 345 of *NATO Advanced Study Institute, Series E*, edited by L. L. Sohn, L. P. Kouwenhoven, and G. Schön (Kluwer, Dordrecht, 1997), p. 105.

[5] R.B. Laughlin, Phys. Rev. Lett. **50**, 1395 (1983).

[6] E. U. Condon and G. H. Shortley, *The Theory of Atomic Spectra* (Cambridge University Press, London, 1935).

[7] D.R. Hartree, Proc. Cambridge Philos. Soc. **24**, 89 (1928).

[8] See, e.g., exact calculations by M. Eto, Jpn. J. Appl. Phys., Part 1 **36**, 3924 (1997); Hartree-Fock calculations by A. Natori, Y. Sugimoto, and M. Fujito, *ibid.* **36**, 3960 (1997); H. Tamura, Physica (Amsterdam) **249B-251B**, 210 (1998); M. Rontani, F. Rossi, F. Manghi, and E. Molinari, Phys. Rev. B **59**, 10 165 (1999); the spin density-functional theory at $B=0$ by In-Ho Lee, V. Rao, R.M. Martin, and J.P. Leburton, *ibid.* **57**, 9035 (1998) and Ref. 43; and also at nonzero B by O. Steffen, U. Rössler, and M. Suhrke, Europhys. Lett. **42**, 529 (1998).

[9] C. Yannouleas and U. Landman, Phys. Rev. Lett. **82**, 5325 (1999).

[10] C. Yannouleas and U. Landman, Phys. Rev. B **61**, 15 895 (2000).

[11] For studies pertaining to the geometrical arrangements of classical point charges in a harmonic confinement, see Yu.E. Lozovik, Usp. Fiz. Nauk **153**, 356 (1987) [Sov. Phys. Usp. **30**, 912 (1987)]; V.M. Bedanov and F.M. Peeters, Phys. Rev. B **49**, 2667 (1994).

[12] For parabolic QD's at zero magnetic field with $6 \leqslant N \leqslant 8$, a crossover from singly humped to doubly humped radial electron densities was found as a function of R_W via path-integral Monte Carlo simulations [R. Egger, W. Häusler, C.H. Mak, and H. Grabert, Phys. Rev. Lett. **82**, 3320 (1999)]. Since the doubly humped radial electron densities are compatible with the $(1,N-1)$ polygonal structures of classical point charges in the range $6 \leqslant N \leqslant 8$ (after carrying out an azimuthal averaging), this crossover was interpreted as indicating the formation of WM's.

[13] These transitions were further elaborated in A.V. Filinov, M. Bonitz, and Yu.E. Lozovik, Phys. Rev. Lett. **86**, 3851 (2001).

[14] C. Yannouleas and U. Landman, Phys. Rev. Lett. **85**, 1726 (2000).

[15] C. Yannouleas and U. Landman, J. Phys.: Condens. Matter **14**, L591 (2002).

[16] C. Yannouleas and U. Landman, Phys. Rev. B **66**, 115315 (2002).

[17] C. Yannouleas and U. Landman, Phys. Rev. B **68**, 035326 (2003).

[18] Unlike the HF approach for which a fully developed theory for the restoration of symmetries has long been established (see Sec. I B), the breaking of symmetries within the spin-dependent density functional theory poses a serious dilemma [J.P. Perdew, A. Savin, and K. Burke, Phys. Rev. A **51**, 4531 (1995)]. This dilemma has not been resolved todate; several remedies (like projection, ensembles, etc.) are being proposed, but none of them appears to be completely devoid of inconsistencies [A. Savin, in *Recent Developments and Applications of Modern Density Functional Theory*, edited by J. M. Seminario (Elsevier, Amsterdam, 1996), p. 327]. In addition, due to the unphysical self-interaction energy (which vigorously and *erroneously* assists the kinetic energy in orbital delocalization), the density functional theory is more resistant against space symmetry breaking [R. Bauernschmitt and R. Ahlrichs, J. Chem. Phys. **104**, 9047 (1996)] than the sS-UHF, and thus it fails to describe a whole class of broken symmetries involving electron localization, e.g., the formation at $B=0$ of Wigner molecules in QD's (see footnote 7 in Ref. 9), the hole trapping at Al impurities in silica [J. Laegsgaard and K. Stokbro, Phys. Rev. Lett. **86**, 2834 (2001); G. Pacchioni, F. Frigoli, D. Ricci, and J.A. Weil, Phys. Rev. B **63**, 054102 (2001)], or the interaction driven localization-delocalization transition in d- and f-electron systems [see, e.g., *Strong Coulomb Correlations in Electronic Structure Calculations: Beyond the Local Density Approximation*, edited by V. I. Anisimov (Gordon & Breach, Amsterdam, 2000); S.Y. Savrasov, G. Kotliar, and E. Abrahams, Nature (London) **410**, 793 (2001)]. In line with the above, no density functional calculations describing space symmetry breaking and formation of Wigner molecules at $B=0$ in *circular* QD's have been reported to date.

[19] Å. Bohr and B.R. Mottelson, K. Dan. Vidensk. Selsk. Mat. Fys. Medd. **27**, No. 16 (1953).

[20] S.G. Nilsson, K. Dan. Vidensk. Selsk. Mat. Fys. Medd. **29**, No. 16 (1955).

[21] K.L. Clemenger, Phys. Rev. B **32**, 1359 (1985).

[22] V.M. Strutinsky, Nucl. Phys. A **95**, 420 (1967); **122**, 1 (1968).

[23] C. Yannouleas and U. Landman, Phys. Rev. B **51**, 1902 (1995).

[24] C. Yannouleas, U. Landman, and R. N. Barnett, in *Metal Clusters*, edited by W. Ekardt (Wiley, Chichester, 1999), p. 145.

[25] P. Ring and P. Schuck, *The Nuclear Many-body Problem* (Springer-Verlag, New York, 1980).

[26] A. Szabo and N. S. Ostlund, *Modern Quantum Chemistry* (McGraw-Hill, New York, 1989).

[27] See in particular Chaps. 5.5 and 11 in Ref. 25. However, our terminology (i.e., UHF vs RHF) follows the practice in quantum chemistry (see Ref. 26).

[28] For the case of high-magnetic fields, see also H.-M. Müller and S.E. Koonin, Phys. Rev. B **54**, 14 532 (1996).

[29] For the restoration of broken rotational symmetries in atomic nu-

clei, see R.E. Peierls and J. Yoccoz, Proc. Phys. Soc. London, Sect. A **70**, 381 (1957), and Chap. 11 in Ref. 25.

[30] For the restoration of broken spin symmetries in natural 3D molecules, see P.O. Löwdin, Phys. Rev. B **97**, 1509 (1955); Rev. Mod. Phys. **36**, 966 (1964).

[31] H. Fukutome, Int. J. Quantum Chem. **20**, 955 (1981), and references therein.

[32] For the restoration of broken spin symmetries in the case of double QD's, leading to a generalized Heitler-London approach for the coupling and dissociation of artificial molecules, see (for $B = 0$) C. Yannouleas and U. Landman, Eur. Phys. J. D **16**, 373 (2001) and (as a function of B); C. Yannouleas and U. Landman, Int. J. Quantum Chem. **90**, 699 (2002).

[33] F. A. Cotton, *Chemical Applications of Group Theory* (Wiley, New York, 1990).

[34] The use of the term yrast is customary in the spectroscopy of rotating nuclei; see, e.g., Å. Bohr and B. R. Mottelson, *Nuclear Structure* (Benjamin, Reading, MA, 1975), Vol. II, p. 41.

[35] S.M. Girvin and T. Jach, Phys. Rev. B **28**, 4506 (1983).

[36] P.A. Maksym and T. Chakraborty, Phys. Rev. Lett. **65**, 108 (1990).

[37] W.Y. Ruan, Y.Y. Liu, C.G. Bao, and Z.Q. Zhang, Phys. Rev. B **51**, 7942 (1995).

[38] T. Seki, Y. Kuramoto, and T. Nishino, J. Phys. Soc. Jpn. **65**, 3945 (1996).

[39] P.A. Maksym, Phys. Rev. B **53**, 10871 (1996).

[40] L. Jacak, P. Hawrylak, and A. Wojs, *Quantum Dots* (Springer, Berlin, 1998), and references therein.

[41] J.A. Pople and R.K. Nesbet, J. Chem. Phys. **22**, 571 (1954); see also, G. Berthier, C. R. Séances Acad. Sci. **238**, 91 (1954).

[42] The UHF equations preserve at each iteration step the symmetries of the many-body Hamiltonian, if these symmetries happen to be present in the input (initial) electron density of the iteration (see Sec. 5.5 of Ref. 25). The input densities into the iteration cycle are controlled by the values of the $P_{\lambda\sigma}^{\alpha}$ and $P_{\lambda\sigma}^{\beta}$ matrix elements. (a) Symmetry-adapted RHF solutions are extracted from Eq. (3) and Eq. (4) by using as input $P_{\lambda\sigma}^{\alpha} = P_{\lambda\sigma}^{\beta} = 0$ for the case of closed shells (with or without an infinitesimally small B value). For open shells, one needs to use an infinitesimally small value of B. With these choices, the output of the first iteration (for either closed or open shells) is the single-particle spectrum and corresponding electron densities at $B = 0$ associated with the Hamiltonian in Eq. (10) (the small value of B mentioned above guarantees that the single-particle total and orbital densities are circular). (b) For obtaining broken-symmetry UHF solutions, the input densities must be different in an essential way from the ones mentioned above. We have found that the choice $P_{\lambda\sigma}^{\alpha} = 1$ and $P_{\lambda\sigma}^{\beta} = 0$ usually produces broken-symmetry solutions (in the regime where symmetry breaking occurs).

[43] M. Koskinen, M. Manninen, and S.M. Reimann, Phys. Rev. Lett. **79**, 1389 (1997).

[44] In some circumstances, SDW's may be obtained from spin density functional calculations (see Ref. 43). In general, however, the breakings of spin and/or spatial symmetries are not properly described within spin density functional theory (see Ref. 18).

[45] The possibility of ground-state configurations with uniform electron density, but nonuniform spin density, was first discussed for 3D bulk metals using the HF method in A.W. Overhauser, Phys. Rev. Lett. **4**, 462 (1960); Phys. Rev. **128**, 1437 (1962).

[46] Depending on the spin polarization, a WM may (or may not) be accompanied by a SDW. Unlike the pure SDW case, however, the SDW of a WM exhibits necessarily the same number of humps as the number of electrons (see, e.g., the case of $N = 3$ electrons in Sec. III B).

[47] However, for $R_W \lesssim 1$, the formation of a special class of SDW's (often called electron puddles) plays an important role in the coupling and dissociation of quantum dot molecules (see Ref. 32 and Ref. 9).

[48] In solid-state physics the Hückel approximation is usually referred to as the tight-binding approximation, with β denoted most often as t [t specifies the tunneling (hopping) between sites].

[49] A. B. Wolbarst, *Symmetry and Quantum Systems* (Van Nostrand Reinold, New York, 1977).

[50] The group theoretical symbol E for the two-dimensional irreducible representations should not be confused with the same symbol denoting the eigenvalues of the Hückel equation or the UHF orbital energies. For the group theoretical symbols, we follow the Schönflies convention. In addition to E, for one-dimensional irreducible representations, we use the capital letters A and B (see Refs. 33 and 49).

[51] P.A. Sundqvist, S.Yu. Volkov, Yu.E. Lozovik, and M. Willander, Phys. Rev. B **66**, 075335 (2002).

[52] S. Hammes-Schiffer and H.C. Andersen, J. Chem. Phys. **99**, 1901 (1993).

[53] E. Brown, Phys. Rev. **133**, A1038 (1964).

[54] J. Zak, Phys. Rev. **134**, A1602 (1964).

[55] R.E. Peierls, Z. Phys. **80**, 763 (1933).

[56] P.G. Harper, J. Phys.: Condens. Matter **3**, 3047 (1991).

[57] R. Kotlyar, C.A. Stafford, and S. Das Sarma, Phys. Rev. B **58**, 3989 (1998).

[58] The RBS wave functions in Eq. (46) work for the group of states that exhibit magic angular momenta and have the lowest possible energy. In our use of the term, the group of these states forms the "yrast" rotational band: namely, the band of states whose excitation energy represents *pure* rotational motion (no other excitations, like center-of-mass motion or vibrational modes, are present).

[59] We note that the *discrete* rotational (and more generally rovibrational) collective spectra associated with symmetry breaking in a QD may be viewed as finite analogs to the Goldstone modes accompanying symmetry-breaking transitions in extended media [see P. W. Anderson, *Basic Notions of Condensed Matter Physics* (Addison-Wesley, Reading, MA, 1984)].

[60] For the appropriate expression of $\mathbf{S}^2$, see Eq. (6) of C. Yannouleas and U. Landman, Int. J. Quantum Chem. **90**, 699 (2002).

[61] Although the wave functions of the Eckardt-frame model are inaccurate compared to the RBS ones [see Eq. (46)], they are able to yield the proper magic angular momenta for (0,N) rings. This result, however, is intuitively built in this model from the very beginning via the phenomenological assumption that the intrinsic wave function, which is never specified, exhibits C_{Nv} point-group symmetries.